J Paleolimnol (2016) 55:319–338
DOI 10.1007/s10933-016-9882-6

ORIGINAL PAPER

Evolving coastal character of a Baltic Sea inlet during the Holocene shoreline regression: impact on coastal zone hypoxia

Wenxin Ning · Anupam Ghosh · Tom Jilbert · Caroline P. Slomp · Mansoor Khan · Johan Nyberg · Daniel J. Conley · Helena L. Filipsson

Received: 30 November 2015 / Accepted: 17 February 2016 / Published online: 25 February 2016

Abstract Although bottom water hypoxia ($O_2 < 2$ mg L^{-1}) is presently widespread in the Baltic Sea coastal zone, there is a lack of insight into past changes in bottom water oxygen in these areas on timescales of millennia, and the possible driving factors. Here, we present a sediment-based environmental reconstruction of surface water productivity, salinity and bottom water oxygen for the past 5400 years at Gåsfjärden, a coastal site in SE Sweden. As proxies, we use dinoflagellate cysts, benthic foraminifera, organic carbon (C_{org}), biogenic silica (BSi), C_{org}/N_{tot}, C_{org}/P_{tot}, Ti/Al, K/Al and grain size distribution. The chronology of the sediment sequence is well constrained, based on ^{210}Pb, ^{137}Cs and AMS ^{14}C dates. Between 3400 and 2100 BCE, isostatic conditions favored enhanced deep water exchange between Gåsfjärden and the open Baltic Sea. At that time, Gåsfjärden was characterized by relatively high productivity and salinity, as well as frequently occurring hypoxic-anoxic bottom water, despite the relatively large connection with the Baltic Sea. The most severe interval of oxygen depletion is recorded between 2400 and 2100 BCE, and appears to coincide

Electronic supplementary material The online version of this article (doi:10.1007/s10933-016-9882-6) contains supplementary material, which is available to authorized users.

W. Ning (✉) · A. Ghosh · M. Khan · D. J. Conley · H. L. Filipsson
Department of Geology, Lund University, Sölvegatan12, 223 62 Lund, Sweden
e-mail: wenxin.ning@geol.lu.se

A. Ghosh
e-mail: anupam.ghosh@gmail.com

M. Khan
e-mail: mansoorswati@yahoo.com

D. J. Conley
e-mail: daniel.conley@geol.lu.se

H. L. Filipsson
e-mail: helena.filipsson@geol.lu.se

A. Ghosh
Center of Advanced Study, Department of Geological Sciences, Jadavpur University, Kolkata 700032, India

T. Jilbert · C. P. Slomp
Department of Earth Sciences, Faculty of Geosciences, Utrecht University, P.O. Box 80.021, 3508 TA Utrecht, The Netherlands
e-mail: tom.jilbert@helsinki.fi

C. P. Slomp
e-mail: c.p.slomp@uu.nl

T. Jilbert
Department of Environmental Sciences, University of Helsinki, P.O. Box 65, 00014 Helsinki, Finland

J. Nyberg
Geological Survey of Sweden, Box 670, 751 28 Uppsala, Sweden
e-mail: johan.nyberg@sgu.se

with a similar hypoxic event in the Gotland Basin in the open Baltic Sea. As regional climate became wetter and colder between 2100 BCE and 700 BCE, salinity declined and bottom water oxygen conditions improved. Throughout the record, grain size, Ti/Al and K/Al data indicate an evolution towards a more enclosed coastal system, as suggested by reconstructions of the post-glacial shoreline regression. Gåsfjärden shifted to close to modern conditions after 700 BCE, and was characterized by less hypoxia and lower salinity compared with 3400–700 BCE. The timing of the shift corresponds with the Sub-Boreal/Sub-Atlantic transition in Europe. Human-induced erosion in the catchment is observed as early as 600 CE, and is particularly prominent since regional copper mining activity increased around 1700 CE. A sharp increase in sediment C_{org} concentration is recorded since the 1950s, indicating significant anthropogenic impact on biogeochemical cycles in the coastal zone, as observed elsewhere in the Baltic Sea.

Keywords Hypoxia · Baltic Sea · Holocene · Biogeochemistry · Dinoflagellate cyst · Coastal zone

Introduction

The Baltic Sea is a semi-enclosed brackish water body connected to the North Sea through the narrow Danish straits. The catchment of the Baltic Sea is ~4 times larger than the sea surface area (392,978 km^2) and is inhabited by more than 85 million people (Leppäranta and Myrberg 2009). Since the 1950s, the use of artificial fertilizers in the catchment increased dramatically and has exerted substantial pressure on the Baltic Sea ecosystem (Emeis et al. 2000; Nehring et al. 1995). Eutrophication is presently a severe problem in the Baltic Sea (HELCOM 2009). Despite large nutrient reductions since the 1980s, which led to an alleviation of eutrophication in many regions and to a healthier Baltic Sea overall (Andersen et al. 2015), winter surface-water phosphate concentrations increased steadily as a result of internal phosphorus loading from sediments and stabilized only in recent years (Emeis et al. 2000; Gustafsson et al. 2012). Nitrogen fixation by cyanobacteria replenishes the nitrogen lost through denitrification and sedimentation (Rolff et al. 2007; Vahtera et al. 2007). The relatively low nitrogen and high phosphorus content in the surface waters further enhance cyanobacteria blooms and contribute to increased eutrophication and oxygen depletion in bottom waters (Vahtera et al. 2007). The modern Baltic Sea environment is well studied, however there is a lack of understanding of how the environment has changed from a long-term perspective, in particular in the coastal zone.

The Baltic Sea transitioned from a freshwater body (Ancylus Lake) to the present brackish system (Littorina Sea) ca. 8000 years ago (Björck 1995). Palaeoecological studies based on sediments from the open Baltic Sea reveal intermittent hypoxic conditions over the last 8000 years, which are linked to changes in climate, stratification, sill depth and anthropogenic activities (Andrén et al. 2000; Jilbert et al. 2015; Jilbert and Slomp 2013; Zillén et al. 2008). Naturally poor ventilation, together with the effects of eutrophication, have resulted in the development of large hypoxic ($O_2 < 1.4$ mL L^{-1} or 2 mg L^{-1}) and anoxic ($O_2 = 0$ mL L^{-1}) areas in the modern Baltic Sea (Carstensen et al. 2014a; Conley et al. 2009). An almost 12-fold increase in the hypoxic area of the Baltic Sea deep basins (from ~5000 to 60,000 km^2) over the last 115 years is reported (Carstensen et al. 2014a), making that part of the Baltic Sea the largest human-induced "dead zone" in the world (Diaz and Rosenberg 2008). Severe hypoxia and anoxia can lead to changes in the benthic community, loss of habitat for benthos and mortality of benthic-dwelling organisms, which influence the ecosystem services provided by the benthic fauna (Carstensen et al. 2014b).

Hypoxia has also increased in coastal areas of the Baltic Sea during recent decades (Conley et al. 2011). Since the 1950s, hypoxic and anoxic conditions expanded significantly in the Archipelago Sea (Bonsdorff et al. 1997), Gulf of Finland (Caballero-Alfonso et al. 2015; Kotilainen et al. 2007), Swedish east archipelagos (Persson and Jonsson 2000; Savage et al. 2010) and Danish coastal areas (Caballero-Alfonso et al. 2015; Conley et al. 2007; Fig. 1). However, compared to the extensively studied deep basins, there are few long-term (>1000 years) environmental reconstructions from the coastal zone that focus on bottom-water oxygen conditions. Because of isostatic rebound, the coastline of the Baltic Sea has evolved continuously throughout the Holocene (Påsse and Andersson 2005). Consequently, locations in the modern coastal zone of the Baltic Sea may have

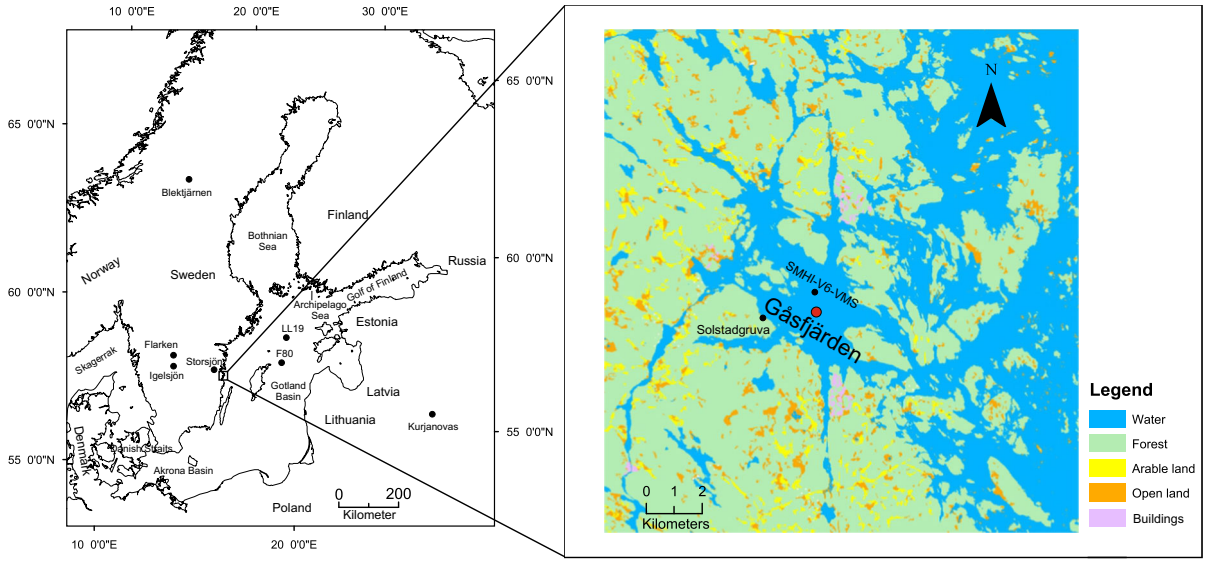

Fig. 1 Location of Gåsfjärden, the coring site (marked with *filled red circle*), the hydrographic monitoring station SMHI-V6-VMS and other sites mentioned in the text. (Color figure online)

experienced pronounced changes in water depth, proximity to land and biogeochemical cycles throughout the Holocene.

In this study, we present a high-temporal-resolution multiproxy reconstruction of productivity, salinity and bottom-water hypoxia in the coastal zone of the Baltic Sea. We show how interactions between isostasy, climate, and land use have impacted the biogeochemistry and phytoplankton composition of the coastal zone over the course of the Holocene. Furthermore, we compare our reconstruction of coastal zone hypoxia with records from the open Baltic Sea.

Site description

Gåsfjärden (57°34′21.3″N, 16°34′58.4″E) is a fjord-like inlet located on the south-east Swedish coast (Fig. 1). It has restricted water exchange with the open Baltic Sea through a narrow and shallow strait ($\sim$500 m wide, <20 m deep) in the east. The coastal sea is characterized by an archipelago with numerous small islands. The area became ice-free ca. 14.5 ka ago (Anjar et al. 2014) and has since then experienced isostatic land uplift (Påsse and Andersson 2005). The surface area of Gåsfjärden is 22 km^2 and the mean and maximum water depths are 10 and 51 m, respectively (SMHI 2003).

Hydrographic variables measured at Gåsfjärden to a maximum of 25 m water depth show strong seasonality (Fig. 2). Monitoring data are sparse for water depths between 0.5 and 20 m, and hence we focused on surface water (0–0.5 m) and bottom water (20–25 m) data. The sea surface temperature is typically 0–5 °C in winter and 15–20 °C in summer. Surface water salinity (2–6) is seasonally variable and bottom water salinity (6–7) is generally stable (Fig. 2). Average surface-water dissolved inorganic nitrogen, phosphate and silicate in winter are 8.5, 0.5 and 66.5 µmol L^{-1}, respectively. Highest chlorophyll *a* values (3–10 µg L^{-1}) are recorded in April. Bottom water is sometimes hypoxic from August to October. A thermocline develops in spring and summer in the region, which prevents mixing (Legrand et al. 2015). Average river inflow into Gåsfjärden is $\sim$10 m^3 s^{-1} (SMHI 2003). Regional phytoplankton composition is dominated by diatoms and dinoflagellates in spring, and small flagellates and cyanobacteria in summer and autumn (Legrand et al. 2015).

The catchment ($\sim$1500 km^2) of Gåsfjärden is characterized by exposed pre-Cambrian bedrock and thin soils (<1 m). Regional vegetation consists mainly of coniferous forest and arable land is sparsely distributed in lowlands (Fig. 1). The catchment is located on the southern rim of a 100,000-km^2 ore-rich geological region of central Sweden (Stephens et al.

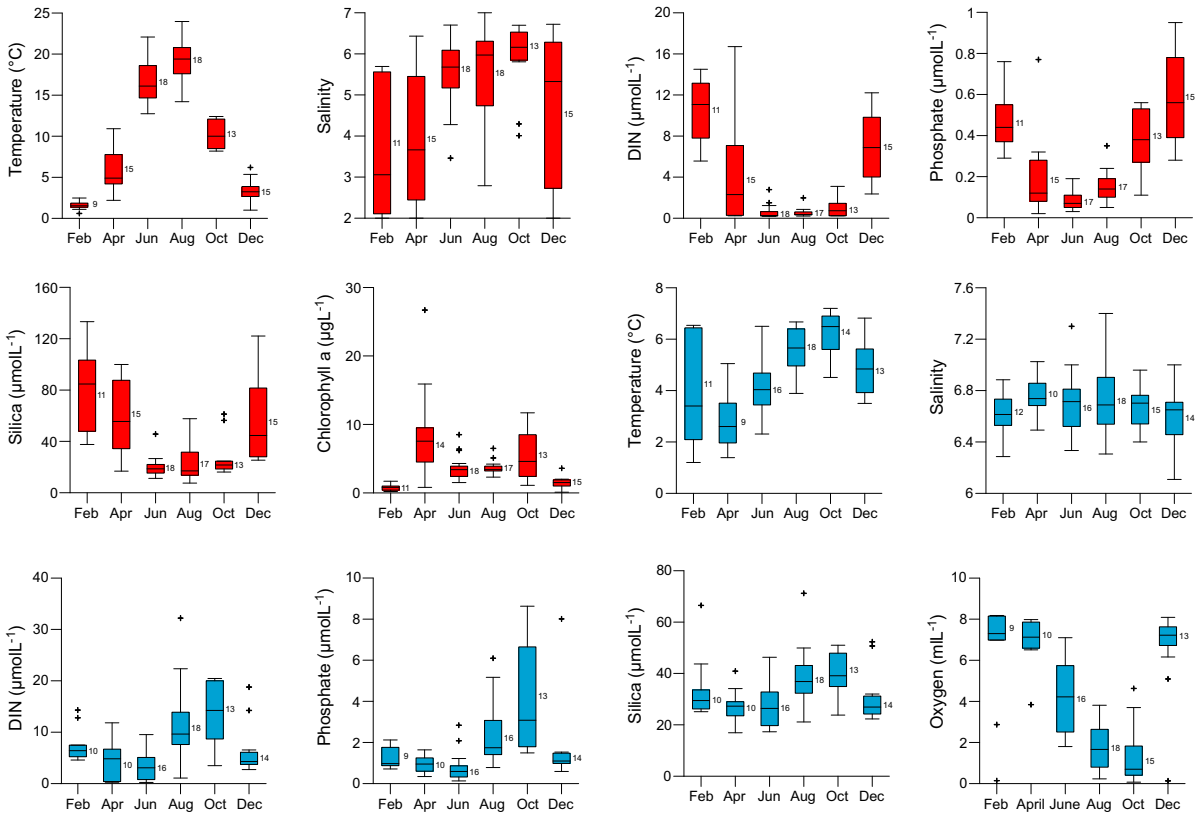

Fig. 2 Hydrographic monitoring data from station SMHI-V6-VMS between the year 1995 and 2012. *Box plots in red* and *blue* represent measurements from surface water (0–0.5 m) and bottom water (20–25 m), respectively. The number of measurements is listed along the *box plots*. DIN is calculated as the sum of nitrate, nitrite and ammonia. The data were measured by the Swedish Meteorological and Hydrological Institute (SMHI). (Color figure online)

2009). Active mining in Solstadgruva, a copper mine along the shore of Gåsfjärden, started in the 1630s and closed in 1919, according to historical documents (Söderhielm and Sundblad 1996). However, small-scale mining could already have occurred in the region by the twelfth to thirteenth centuries, as suggested by sedimentary metal concentrations (Karlsson et al. 2015).

Materials and methods

Core collection and sediment subsampling

Sediment cores were collected at Station VG31 (56°34′23″N, 16°31′26″E) in August, 2011 from the *R/V Ocean Surveyor* (Fig. 1). The water depth at the coring site is 31.2 m. Two piston cores $VG31L_{UU}$ (560 cm long) and $VG31L_{LU}$ (576 cm long), and several short Gemini cores (~50 cm) were retrieved (Table 1). Long core $VG31L_{LU}$ was cut into six 1-m-long segments, split lengthwise, photographed and documented on board. At the Department of Geology in Lund University, Sweden, half of long core $VG31L_{LU}$, and short cores $VG31D_{LU}$ and $VG31F_{LU}$, were sliced into 1-cm intervals and freeze-dried. The other half of $VG31L_{LU}$ is archived at +4 °C at Lund University. At the Department of Earth Sciences in Utrecht University, The Netherlands, long core $VG31L_{UU}$ and frozen short core $VG31S_{UU}$ were subsampled. Subsamples of long core $VG31L_{UU}$ were taken at intervals of 4–5 cm in the lower 300 cm where distinct laminations were visible. The top 250 cm of sediment core $VG31L_{UU}$ was sampled every 10 cm. Frozen short core $VG31S_{UU}$ was subsampled at intervals of 2 cm.

Table 1 Description of sediment cores and corresponding analysis

Sediment core	Core type	Length (cm)	Analysis
$VG31D_{LU}$	Gemini	52	C_{org}, N_{tot}, Dinoflagellate cyst, foraminifera, grain size
$VG31F_{LU}$	Gemini	55	^{210}Pb, ^{137}Cs, C_{org}
$VG31S_{UU}$	Gemini	60	C_{org}, N_{tot}, ρ_{dry}, total elemental composition (HF destruction and ICP-OES)
$VG31L_{LU}$	Piston	578	C_{org}, N_{tot}, Dinoflagellate cyst, foraminifera, grain size, ^{14}C dating
$VG31L_{UU}$	Piston	560	C_{org}, N_{tot}, ρ_{dry}, total elemental composition (HF destruction and ICP-OES)

Chronology

The age-depth model was established using ^{210}Pb and accelerator mass spectrometry (AMS) radiocarbon ^{14}C dating techniques. The ^{137}Cs peak measured in the upper sediments was used as a marker of the Chernobyl reactor accident in 1986. The ^{210}Pb dating was performed at the Department of Geology, Lund University. Seven mollusk shell samples and nine terrestrial plant fragments were radiocarbon-dated at the Radiocarbon Dating Laboratory of Lund University (Table 2). The age-depth model from ^{14}C dates was obtained using the software OxCal v4.1.7 (Ramsey 2008). Before the age-depth calibration, reservoir age (R) was estimated through $\delta^{18}O$ measurements on *Macoma balthica* shells, according to the regional calibration by Lougheed et al. (2013), expressed as $R = 41.8 \times \delta^{18}O + 390$ (Table 3).

Organic carbon and nitrogen

Sediment organic carbon (C_{org}) and nitrogen content were analyzed following the methods of Verardo et al. (1990) and Van Santvoort et al. (2002). At Lund University, dried sediment was transferred into a silver (Ag) capsule and moistened. Subsequently 10 % HCl was added to each sample, with the samples heated on an aluminum plate at 50 °C. The samples were dried on the plate and the tin (Sn) capsules were wrapped along with the dried Ag capsules. The samples were analyzed using an elemental analyzer (Costech ECS 4010). At Utrecht University, samples were first decalcified by adding 1 M HCl for 12 and then 4 h. The samples were then analyzed using an elemental analyzer (Fison Instruments, NA 1500 NCS). The mass accumulation rate (MAR) of C_{org} was calculated as follows: C_{org} MAR = C_{org} (%) × sedimentation rate × ρ_{dry}, where ρ_{dry} corresponds to the bulk density of samples.

Core correlation

The sediment core C_{org} concentrations (Table 1) were used for core correlation. Correlation between short core $VG31D_{LU}$ and long core $VG31L_{LU}$ was satisfactory [$r = 0.91$, $p < 0.01$; Electronic Supplementary Material (ESM) Fig. 1] and suggests an overlap of 21 cm between the short core and the long core. The C_{org} values from $VG31S_{UU}$ correlate well with $VG31D_{LU}$ ($r = 0.92$, $p < 0.01$) after correction for the expansion of $VG31S_{UU}$ during freezing (ESM Fig. 2). The highly correlated C_{org} values ($r = 0.87$, $p < 0.01$) from $VG31D_{LU}$ and $VG31F_{LU}$ indicate that the two cores have a similar age-depth relationship (ESM Fig. 3). The correlation between long cores $VG31L_{LU}$ and $VG31L_{UU}$ is also satisfactory ($r = 0.89$, $p < 0.01$; ESM Fig. 4). As the chronology was established based on the sediment sequence analyzed at Lund University, the sediment core depth from Lund University was used to establish the composite core depth. The sediment core depth from Utrecht University was transferred to the composite core depth from Lund University.

Biogenic silica analysis

Biogenic silica (BSi) analysis was performed at the Department of Geology, Lund University. The extraction of biogenic silica used a weak-base method in which alumino-silicates release silica linearly over time and most BSi dissolves completely in the first 2 h of the digestion (DeMaster 1981). Approximately 30 mg of sediment was mixed with 40 mL of 0.094 M Na_2CO_3 solution and digested for 5 h at 85 °C. 1-mL aliquots were removed from each sample after 3, 4 and

Table 2 Descriptions of the dated materials and the dating results

Sample code	Composite core depth (cm)	Lab. No.	Material	Weight (mg)	^{14}C date (BP)	Applied reservoir age	Calibrated age in 2σ (CE/BCE)
VG31D-40	40	LuS 9843	Plant remains	5.9	325 ± 45	0	1560 ± 57 CE
VG31L-22	51	LuS 10719	Plant remains	4.9	280 ± 40[a]	0	1597 ± 78 CE
VG31L-40	69	LuS 9844	Plant remains	6.5	370 ± 50	0	1539 ± 60 CE
VG31L-60	89	LuS 9845	Plant remains	18.6	680 ± 50	0	1324 ± 44 CE
VG31L-76	105	LuS 9846	Plant remains	4.5	1015 ± 50	0	1030 ± 64 CE
VG31L-138	167	LuS 10708	Plant remains	1.2	1675 ± 50	0	365 ± 68 CE
VG31L-223	252	LuS 10709	Plant remains	2.5	2655 ± 45	0	833 ± 37 BCE
VG31L-243	272	LuS 10710	Plant remains	1.8	2945 ± 50	0	1151 ± 78 BCE
VG31L-282	311	LuS 10711	Plant remains	5.2	3310 ± 45	0	1590 ± 60 BCE
VG31L-336	365	LuS 9523	Shell (*Macoma balthica*)	111.5	3740 ± 50	300	1870 ± 74 BCE
VG31L-371	400	LuS 9847	Shell (*Macoma balthica*)	26.5	3960 ± 50	300	2178 ± 85 BCE
VG31L-402	431	LuS 9848	Shell (*Mytilus edulis*)	18.5	4070 ± 50	300	2346 ± 80 BCE
VG31L-436	465	LuS 10723	Shell (*Macoma balthica*)	3.9	4275 ± 40	300	2498 ± 62 BCE
VG31L-493	522	LuS 9524	Shell (*Macoma balthica*)	4.5	4805 ± 50[a]	300	3374 ± 118 BCE
VG31L-546	575	LuS 10724	Shell (*Mytilus edulis*)	4.6	4805 ± 40	300	3214 ± 83 BCE
VG31L-576	605	LuS 10725	Shell (*Macoma balthica*)	1.8	4820 ± 70	300	3215 ± 117 BCE

[a] Samples recognized as outliers and not used in the age-depth model

Table 3 Estimation of reservoir ages based on δ^{18}O measurements fom *M. balthica* shell remains

Sample code	Composite core depth (cm)	δ^{18}O (V-PDB)	Estimated reservoir age
VG31L 336	365	−2.42	289
VG31L 342	371	−2.19	298
VG31L 371	400	−2.28	295
VG31L 493	522	−2.00	307

5 h. Dissolved silicate was determined by the molybdate blue spectrophotometric method. The weight percentages of BSi at 3, 4 and 5 h are plotted versus time, and the extrapolated intercept value at time zero is the BSi content of the sample (DeMaster 1981). The MAR of BSi was calculated as BSi MAR = BSi (%) × sedimentation rate × ρ_{dry}.

Total sediment composition

To determine total concentrations of elements in the sediment, 0.125 g of sample from selected depths was dissolved in 2.5 mL of 40 % HF, and 2.5 mL of a 72 % $HClO_4$ and 65 % HNO_3 mixture (volumetric ratio 3:2) in closed Teflon bombs at 90 °C, followed by evaporation of the solution and redissolution of the remaining gel in 1 M HNO_3. Concentrations of P, K, Mo, Al and Ti in the HNO_3 solutions were analyzed with inductively coupled plasma optical emission spectroscopy (ICP-OES).

Grain size analysis

Prior to the grain size analysis, organic matter, carbonate and BSi were removed from the sediments using the procedures of Van Hengstum et al. (2007). To obtain enough minerogenic material, about 13 g of mixed sediment sample, each containing a maximum of 7 cm of core section, were used for individual analysis. To remove organic matter and carbonate, 33 % H_2O_2 and 10 % HCl were used, respectively. To remove BSi, the sample was boiled in 100 mL of 8 % NaOH. Sand particles (>63 μm) were sieved, dried and weighed. The mass fraction of sand was calculated

by dividing the dried sand weight by the original dry sample weight before chemical treatment. The mass fraction of clay (<2 μm) and silt (2–63 μm) from particles <63 μm were obtained with a Micromeritics Sedigraph III Particle Size Analyser at the Department of Geology, Lund University.

Microfossil analysis

For dinoflagellate cyst analysis, samples were processed following the guidelines of Rochon et al. (1999), Pospelova et al. (2010) and Zonneveld et al. (2012). Prior to chemical treatment, two tablets of calibrated *Lycopodium clavatum* spores were added to about 0.3 g of sediment. The samples were first treated with 10 % HCl and then soaked in 48 % HF for 2 days after which the samples were neutralized by rinsing with distilled water. The residues after treatment were rinsed through 125 and 20 μm sieves. The residues between 20 and 125 μm were then sonicated gently for up to 60 s before sieving with 20 μm again. Organic-walled microfossils were identified by light microscopy (magnification 600×), following Rochon et al. (1999). The concentrations of the microfossils were calculated and expressed as amounts of individuals per gram (Benninghoff 1962). For foraminiferal analysis, 1 g of dry sediment was wet-sieved with 100 and 45 μm sieves. Residues larger than 45 μm were analyzed using a binocular stereo zoom microscope (Nikon SMZ 1500).

Zonation of proxy variables

Stratigraphically constrained cluster analysis was applied to distinguish geochemical (GEO) and biological (BIO) zones, using the incremental sum of squares method (Grimm 1987). The analysis was carried out using the R package rioja (Juggins 2014). Geochemical proxies used in the cluster analysis were C_{org}, BSi, C_{org}/N_{tot} and the clay fraction (measured at Lund University), and C_{org}/P_{tot}, K/Al and Ti/Al (measured at Utrecht University). The benthic foraminifera and the dinoflagellate cyst *Ataxiodinium choane* were excluded in the zonation of biological proxies because of their low occurrence.

Results

Chronology

Unsupported ^{210}Pb activity shows a decreasing trend with depth in the sediments of the short core $VG31F_{LU}$ over the upper 20 cm of the sediment (Fig. 3). Equilibrium between total ^{210}Pb activity and supported ^{210}Pb activity (measured as ^{226}Ra) is reached at ~12 cm. The top 12 cm correspond to the years 1922–2011 according to the constant rate of supply (CRS) model. Peak ^{137}Cs activity is recorded at 5–6 cm sediment depth, and was a consequence of the Chernobyl reactor accident (Zalewska and Suplińska 2013). This sediment interval is dated to 1987–1991 CE using ^{210}Pb. Linear sedimentation rate increases from 0.1 to 0.15 cm a^{-1} between 1943 and 1999 to 0.3–0.6 cm a^{-1} between 1999 and 2010, implying a transition to more unconsolidated sediment at the core top.

Estimated local reservoir ages are between 289 and 307 years, based on δ^{18}O measurements from shell remains of *M. balthica* (Table 3). A 300-year reservoir age was subtracted from the ^{14}C dates of shell samples before establishing the age-depth model. The established chronology suggests that the sediment sequence from Gåsfjärden covers the last 5400 years (Fig. 3). Sedimentation rates are about 0.15 cm a^{-1} between 3400 and 1600 BCE and 0.1 cm a^{-1} between 1600 BCE and 1940 CE.

Sediment lithology

X-ray images show that the sediment is laminated throughout nearly the entire 605-cm record (Fig. 4). This primary laminated structure indicates a generally low degree of bioturbation. Traces of bioturbation can be observed at certain intervals in the X-ray image, such as at ~520 cm, where shell fragments were also encountered. The thickness of laminae, based on X-ray images from the entire sediment sequence, varies from several mm to >10 mm. Considering that the sedimentation rate is generally less than 0.15 cm a^{-1}, this suggests that the structures are not annual laminations (varves). The laminations reflect changes in the depositional regime that occurred over a period of years to decades, or rapid events linked with storms.

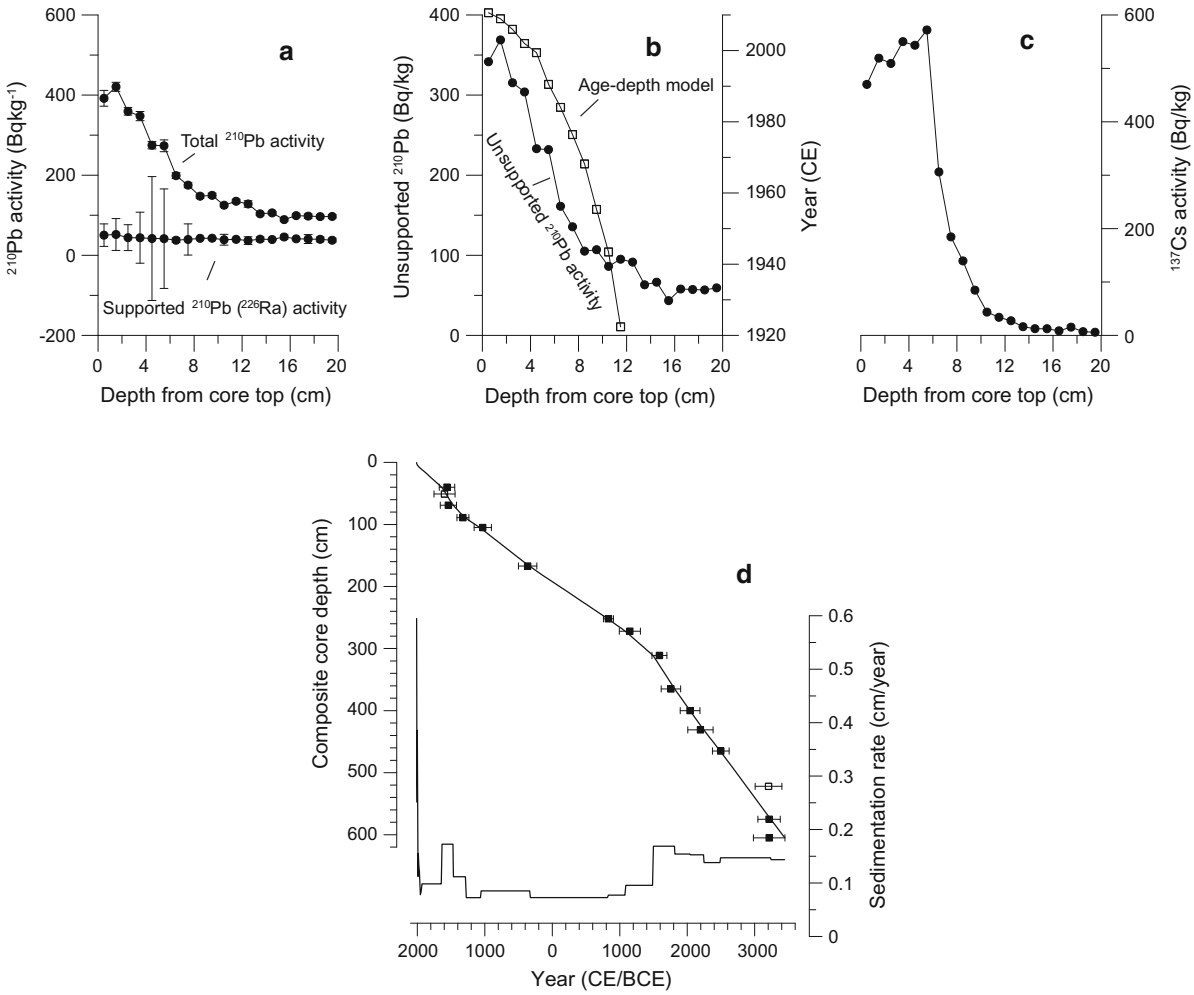

Fig. 3 Age-depth calibration for the sediment sequence from Gåsfjärden. **a** Total and supported ^{210}Pb activities; **b** unsupported ^{210}Pb activity and the associated age-depth model; **c** measured ^{137}Cs activity; **d** age-depth model for the whole sediment sequence based on both ^{210}Pb and ^{14}C dates and calculated sedimentation rates

A secondary source of laminations is observed in the banded coloration of the sediment, as observed in the core photographs taken on board (Fig. 4). In some intervals, this banding correlates with the underlying primary laminated structure, but in others the colored banding is absent whereas the laminations can still be detected in the X-ray images. The light–dark banding is most pronounced between 605 and 265 cm. Above 265 cm, the sediments become generally lighter and the banding is less apparent.

Dinoflagellate cysts and benthic foraminifera

Dinoflagellate cyst species recorded from the Gåsfjärden sediment cores include *Operculodinium centrocarpum* (Wall and Dale 1968), *Pyxidiniopsis psilata* (Head 1994), *Spiniferites* spp. (Wall and Dale 1968), *Lingulodinium machaerophorum* (Deflandre and Cookson 1955) and *Ataxiodinium choane* (Reid 1974). Benthic calcareous foraminifera, including *Cribroelphidium albiumbilicatum*, *Haynesina germanica* and *Ammonia* sp., were grouped together because of their limited abundance. Abundances of microfossils are separated into two major zones and four subzones (Fig. 5).

Zone BIO-A1 (3400–2100 BCE)

The zone is characterized by high concentrations of dinoflagellate cysts (42,000–90,000 cysts g^{-1}) and

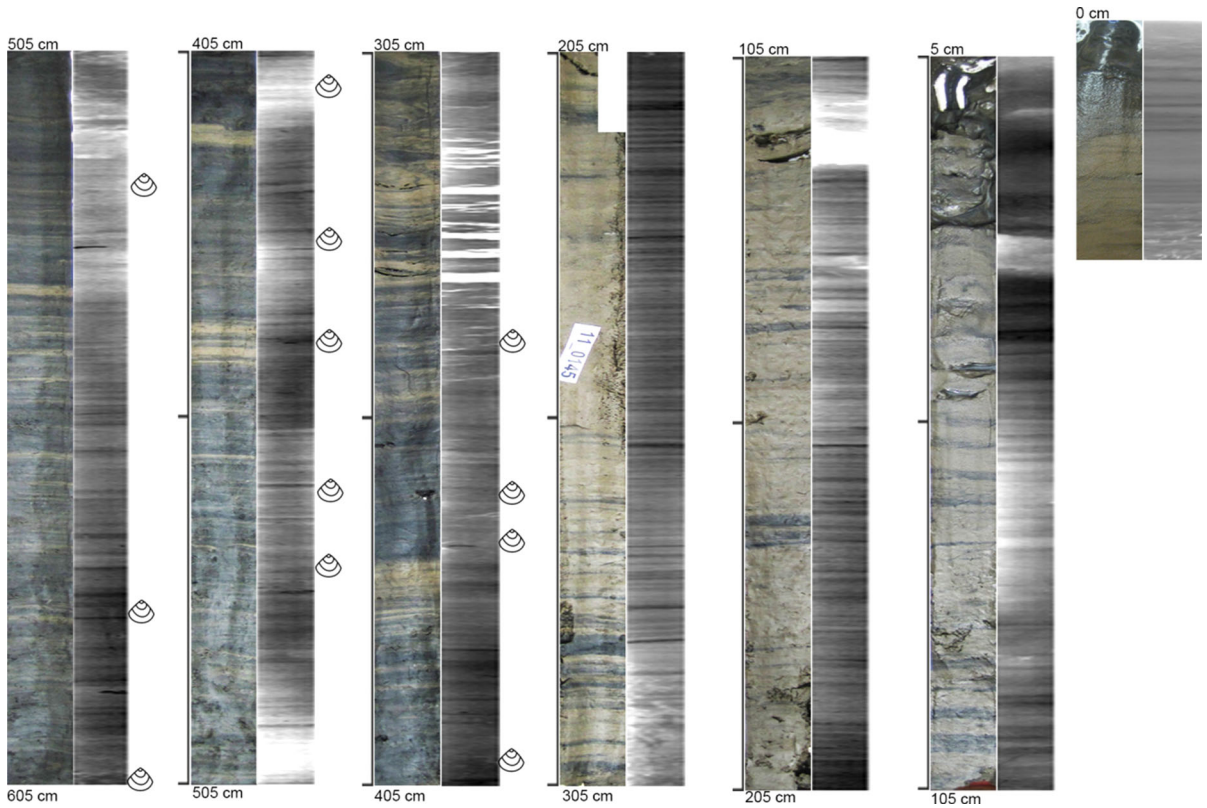

Fig. 4 Optical and X-ray images of the sediment sequence retrieved from Gåsfjärden, showing the lithology. Of the paired images, *pictures on the left* and *right* show photos taken on board after opening the piston core and X-ray images, respectively. *Shell symbols* indicate the location where shell fragments were encountered

the presence of benthic foraminifera. *Operculodinium centrocarpum* is the dominant species and its abundance ranges between 24,000 and 40,000 cysts g^{-1}. The *P. psilata* abundance exhibits large fluctuations (5000–30,000 cysts g^{-1}) and higher concentrations are recorded at 3100 and 2700 BCE. The *Spiniferites* spp. abundance fluctuates between 11,000 and 25,000 cysts g^{-1} and the *L. machaerophorum* abundance ranges from 2000 to 4000 cysts g^{-1}. There is limited occurrence of *A. choane* in this zone. Calcareous benthic foraminifera are present in the lower part of this zone, between 3400 and 3000 BCE, and are not observed elsewhere in the record.

Zone BIO-A2 (2100–700 BCE)

Abundances of the microfossils generally decrease in this zone. The *O. centrocarpum* abundance varies from 10,000 to 50,000 cysts g^{-1} between 2100 and 1400 BCE, and a continuous decrease is observed from 1300 BCE onwards. The *P. psilata* and *Spiniferites* spp. abundance decreases to less than 5000 and 5000–15,000 cysts g^{-1} respectively, much lower than in Zone BIO-A1. The *L. machaerophorum* abundance is also generally lower compared with Zone BIO-A1, especially after 1900 BCE.

Zone BIO-B1 (700 BCE–1200 CE)

The boundary at the transition from BIO-A2 to BIO-B1 marks a significant environmental change based on the dinoflagellate cyst data. This zone is characterized by low *O. centrocarpum* abundance (5000–15,000 cysts g^{-1}), low *Spiniferites* spp. abundance (<5000 cysts g^{-1}) and few *P. psilata* and *L. machaerophorum*.

Zone BIO-B2 (1200–2000 CE)

The *O. centrocarpum* (10,000–25,000 cysts g^{-1}) and *P. psilata* abundances (2500–7500 cysts g^{-1}) are

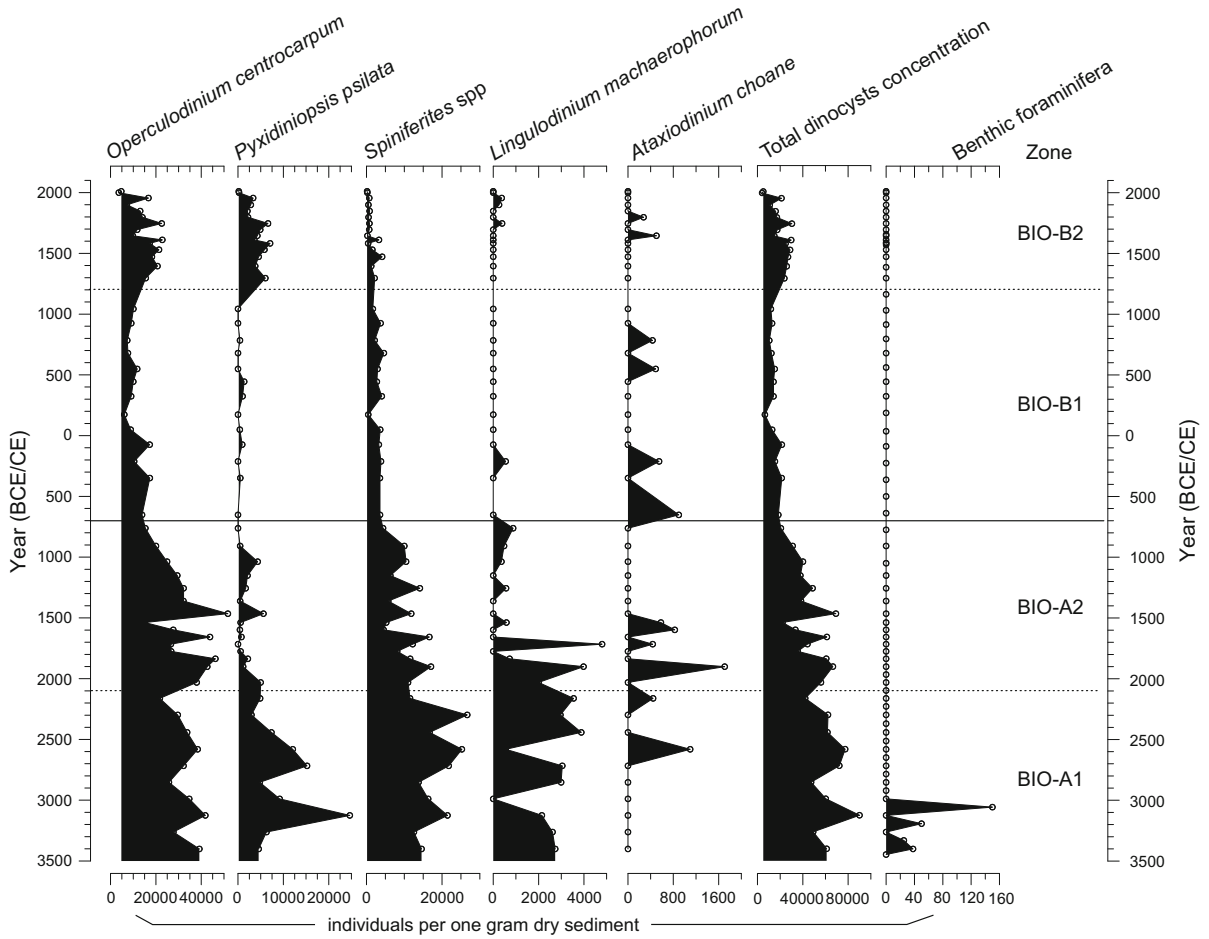

Fig. 5 Concentrations of microfossils, including dinoflagellate cysts and benthic calcareous foraminifera plotted versus age. Microfossil zones are shown

elevated in this zone compared with the previous zone. The *Spiniferites* spp. abundances become lower than in *Zone BIO-B1*. The abundances of *L. machaerophorum* and *A. choane* are consistently low.

Geochemistry

Cluster analysis on C_{org}, BSi, C_{org}/N_{tot}, C_{org}/P_{tot}, K/Al, Ti/Al and grain size data indicates two major zones and five subzones (Fig. 6).

Zone GEO-A1 (3400–2100 BCE)

C_{org} contents (7–11 %) show an increasing trend from 3400 BCE onwards, whereas the C_{org} MAR is rather constant, at about 40 g m^{-2} a^{-1} (Fig. 6). The BSi values are ~20 % between 3400 and 3000 BCE and decrease to 15 % at 2300 BCE. An increase of BSi to 20 % between 2300 and 2100 BCE is observed. The BSi MAR ranges from 74 to 92 g m^{-2} a^{-1} between 3400 and 3000 BCE and decreases to 50–73 g m^{-2} a^{-1} between 3000 BCE and 2100 BCE. C_{org}/N_{tot} values (6–6.5) are stable. Despite large variations in certain intervals, the C_{org}/P_{tot} values mostly range between 200 and 275 and are consistently >250 between 2400 and 2100 BCE. Both K/Al (0.39–0.40) and Ti/Al (0.047–0.049) exhibit declines in this zone. Although clay is dominant in the <63-μm size fraction, the zone has a relatively lower clay fraction (75–78 %) in the record. Silt (22–25 %) and sand fractions (0.2–0.6 %) are relatively high in this zone.

Zone GEO-A2 (2100–700 BCE)

C_{org} values decrease gradually from 11 to 9 % and the C_{org} MAR decreases from 40 to 20 g m^{-2} a^{-1} at 1500 BCE. The BSi values decrease from 17 to 14 % between 2100 and 1500 BCE and slightly increase after 900 BCE. At the same time BSi MAR decreases from 70 g m^{-2} a^{-1} at 2100 BCE to 25 g m^{-2} a^{1} in 1500 BCE and the values show little variability thereafter. C_{org}/N_{tot} values are higher in the zone compared to Zone GEO-A1 and increase to 6.5 at 1500 BCE. The C_{org}/P_{tot} ratios exhibit a decline in this zone, with values between 250 and 180. Both K/Al (0.375–0.39) and Ti/Al (0.046–0.047) exhibit a decreasing trend in this zone. Clay fractions increase from 76 to 80 %, whereas silt fractions decrease from 24 to 20 %. Sand fractions ($\sim$0.2 %) are consistently low.

Zone GEO-B1 (700 BCE–600 CE)

The main zonation boundary for the transition from GEO-A2 to GEO-B1 was at 700 BCE. In zone GEO-B1, C_{org} values ($\sim$9 %) and C_{org} MAR (13–20 g m^{-2} a^{-1}) are generally stable. BSi values decrease almost linearly from 20 to 14 % and BSi MAR (24–33 g m^{-2} a^{-1}) is stable. There is no significant change observed from the C_{org}/N_{tot} values ($\sim$6.5). C_{org}/P_{tot} show rather consistent values around 160 and are lower than in GEO-A2. Minor fluctuations are observed from the K/Al ($\sim$0.375) and Ti/Al ($\sim$0.046). Clay and silt fractions are stable, at about 81 and 19 %, respectively. Sand ($\sim$0.15 %) fractions are low.

Zone GEO-B2a (600–1700 CE)

C_{org} decreases in this zone to 7 %. C_{org} MAR exhibits a slight increase at 1500–1600 BCE. BSi (10–16 %) decreases with minor fluctuations. BSi MAR values slightly increase to above 40 g m^{-2} a^{-1} at ca. 1500 BCE. A slight increase is recorded in the C_{org}/N_{tot} ratios. C_{org}/P_{tot} ratios decrease to as low as 150. Both K/Al and Ti/Al are slightly elevated in this zone compared with the previous zone. Clay (80–83 %) and silt (17–20 %) fractions exhibit larger fluctuation compared with Zone GEO-B1. Sand fractions slightly increase around 1200 and 1500 CE.

Zone GEO-B2b (1700–2010 CE)

A slight decrease of C_{org}, from 7 to 6 %, is observed between 1700 and 1950. However, since the 1950s the C_{org} values show a substantial increase. C_{org} MAR is below 20 g m^{-2} a^{-1} before the 1950s, but the values

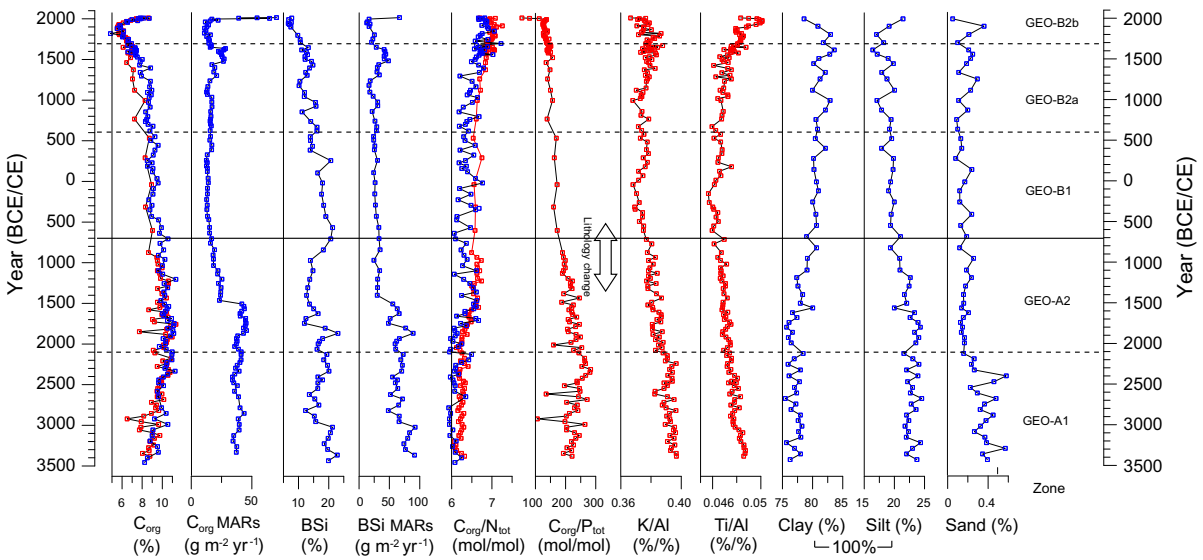

Fig. 6 Geochemical variables plotted as a function of age. *Blue* and *red circles* represent measurements from Lund University and Utrecht University, respectively. The *arrow* in the panel of the C_{org}/P_{tot} data indicates the interval at which the lithology gradually changes from sediments with distinct banding to more homogenous sediments. (Color figure online)

increase sharply thereafter. BSi decreases from 12 % at 1700 CE to the lowest values of 6 % in the record since 1900 CE. BSi MAR is about 15 g m^{-2} a^{-1}, and a high value of 67 g m^{-2} a^{-1} is recorded at the sediment surface. C_{org}/N_{tot} ratios (~7) are at the highest values of the record. C_{org}/P_{tot} continuously decreases, with a significant drop after 2000 CE. K/Al ratios decrease slightly from 0.38 to 0.37 in this zone. Ti/Al increase in this zone and a peak is observed around 1950 CE. There are only three samples with grain size analysis in this zone, but an increasing content of the silt fraction (17–21 %) is recorded.

Discussion

Past environmental changes in Gåsfjärden

The cluster analysis divides the biological and geochemical variables into a similar set of zones, particularly in the early part of the records (Figs. 5, 6). This indicates that ecological transitions in Gåsfjärden were closely connected to changes in the biogeochemistry of the inlet. We consider a four-stage evolution of Gåsfjärden during the Holocene regression, from a relatively offshore system to one with the highly coastal character observed today.

Stage 1 (3400–2100 BCE): Open, productive, high salinity and frequent hypoxia

During Stage 1, relative sea level was 12–18 m above present sea level (Påsse and Andersson 2005), and Gåsfjärden was relatively well-connected to the open Baltic Sea (Fig. 7). Taking the 6 m accumulation of sediments into consideration, the water depth at our coring site was about 55 m at 3400 BCE (Fig. 8). As a consequence of the higher openness and higher sea level, the cross-sectional area of the sills between Gåsfjärden and the open sea was larger than at present, resulting in more efficient deep-water exchange.

The dinoflagellate cyst composition during Stage 1 is similar to records from the southern Baltic Sea and the Gotland Basin (Brenner 2005; Yu and Berglund 2007), and is dominated by the euryhaline species of *O. centrocarpum* (Willumsen et al. 2013). Relatively high abundances of *Spiniferites* spp. and *L. machaerophorum* suggest that this stage has the highest surface salinity in our sediment record (Sildever et al. 2015; Willumsen et al. 2013). Previous reconstructions also indicate a relatively high salinity (10–12) between 4000 and 2000 BCE in the Baltic Sea (Gustafsson and Westman 2002; Ning et al. 2015; Widerlund and Andersson 2011). It is believed that *P. psilata* represents the ecophenotypic form of *O. centrocarpum* in a low-salinity environment (Dale 1996). The highest concentration of *P. psilata* in our study was recorded at 3100 BCE and this event was also recorded in the Gotland Basin (Brenner 2005). Finding benthic calcareous foraminifera in this zone, between 3400 and 3000 BCE, suggests a bottom-water salinity of at least 13–14, based on the modern-day distribution of benthic foraminifera (Hermelin 1987). Based on the surface and bottom water salinity estimates, it is likely that a halocline was present at our coring site (Fig. 8).

High C_{org} and BSi contents and MARs between 3400 and 2100 BCE indicate a highly productive environment during Stage 1. The C_{org}/N_{tot} ratios (~6.5) are close to the Redfield ratio of 106:16, indicating phytoplankton as the dominant source of organic matter (Meyers 1994; Redfield 1963).

High C_{org}/P_{tot} ratios (>200), indicative of enhanced release of phosphorus from sediment relative to organic carbon, imply a hypoxic bottom-water environment (Algeo and Ingall 2007; Conley et al. 2009; Jilbert and Slomp 2013). Dark bands in the core lithology, which are likely stained with sulfide, also support this interpretation. We note that sediment Mo/Al ratios remain below 0.0006 (typically between 0.0001 and 0.0002) throughout the record (ESM Table 1). These values are well below those reported for the deep basins of the open Baltic Sea today (Jilbert and Slomp 2013), and are consistent with hypoxic, but not euxinic (sulfidic) depositional conditions. Climate reconstructions indicate that warmer (1.5–2.5 °C) and drier conditions prevailed between 3400 and 2100 BCE (Hammarlund et al. 2003; Heikkilä and Seppä 2010; Seppä et al. 2005). Such conditions may have favored phytoplankton production (Blass et al. 2007; Sun et al. 2011) and cyanobacteria growth (Funkey et al. 2014; Vahtera et al. 2007). Excess release of phosphorus from sediments would be expected to further enhance the growth of cyanobacteria by stimulating nitrogen fixation (Vahtera et al. 2007). During Stage 1, C_{org}/P_{tot} values varied between 200 and 280. This suggests the existence of intervals with less oxygen-depleted bottom water, which might be

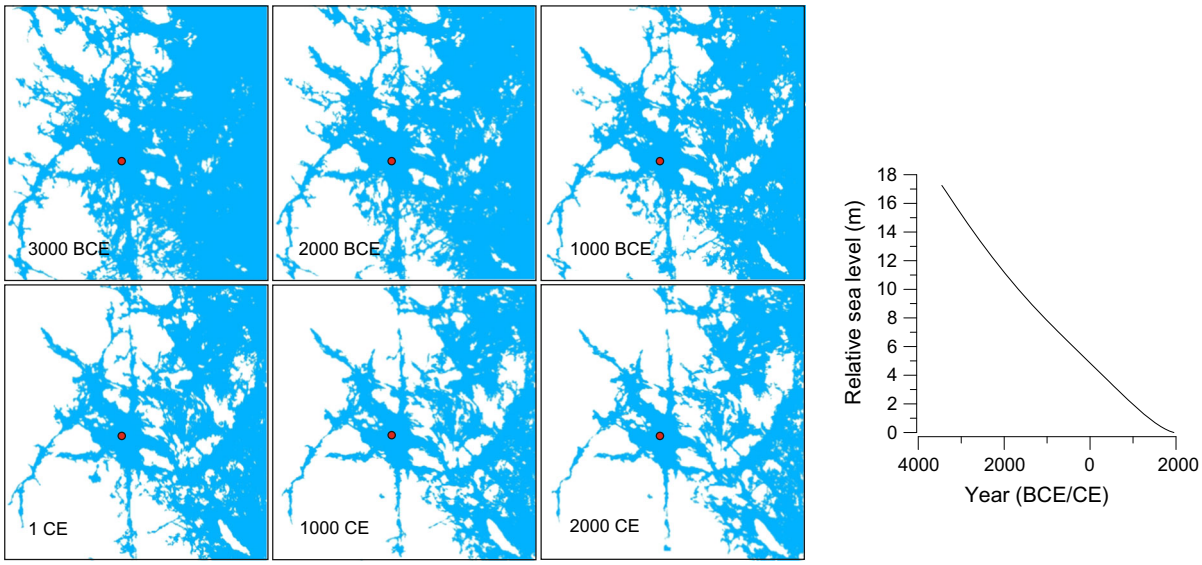

Fig. 7 Geomorphology variations of Gåsfjärden (*left*) associated with the relative sea level change over time (*right*). The relative sea level curve is based on Påsse and Andersson (2005). *Red circle* represents the coring location. (Color figure online)

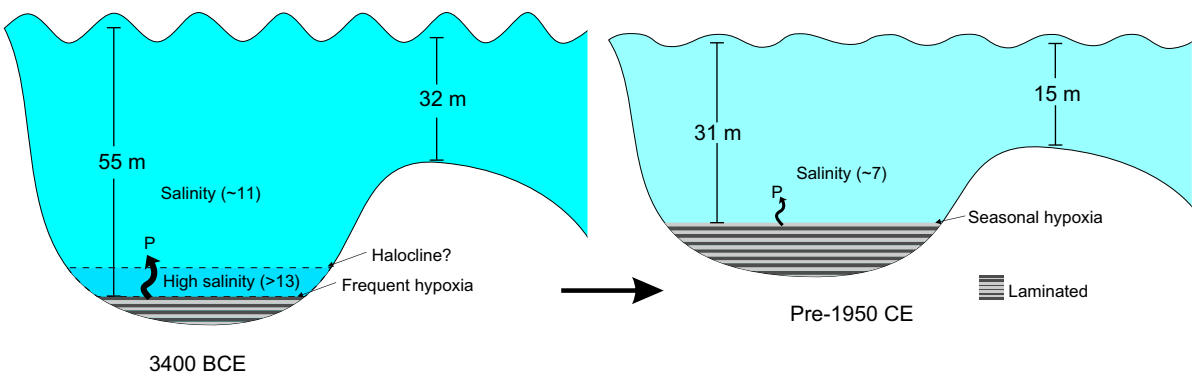

Fig. 8 Conceptual illustrations showing the environment of Gåsfjärden at 3400 BCE and pre-1950 CE. Phosphorus released relative to C_{org} from sediment was stronger at 3400 BCE compared with pre-1950 CE

caused by temporary climate shifts to wetter/colder conditions. For example, relatively low C_{org}/P_{tot} values in this stage are recorded at 3000 BCE, corresponding with temporary cooling (Seppä et al. 2005; Fig. 9).

The detrital component of the sediment during Stage 1 was relatively coarse-grained, with the highest fractions of sand observed at any time during the Holocene (Fig. 6). Along the east coast of Sweden today, a band of sandy sediments is observed directly offshore, whereas enclosed bays such as Gåsfjärden are characterized by clay-rich mud (Al-Hamdani and Reker 2007). This pattern reflects the energy regimes of different parts of the coastal zone, whereby muddy sediment is more likely to accumulate in sheltered inshore locations. We propose that during Stage 1, when the study site was located further offshore, a higher-energy sedimentation regime was active, which led to the accumulation of proportionally more sand-size particles.

The chemical composition of the detrital component of the sediments was also distinctly different during Stage 1 compared to the rest of the record, with relatively high K/Al and Ti/Al ratios at that time. High K/Al in marine sediments is indicative of a high proportion of illite (Wehausen and Brumsack 2000), a

K-rich glacial clay that is widely distributed in the Baltic region (Gingele and Leipe 1997; Virtasalo et al. 2011). Hence, despite the generally lower proportion of clay during Stage 1, the composition of the clay fraction was more illite-dominated than during later intervals. Illite is typically the dominant mineral in the size fraction <2 μm in the Gotland Basin of the open Baltic Sea (Emel'yanov and Luksha 2014). We interpret the high K/Al of Stage 1 to indicate the dominance of a regional (Baltic-wide) clay mineral assemblage over a local signal from the catchment of Gåsfjärden itself. The co-variance of Ti/Al with K/Al supports the conclusion that the composition of detrital material has varied through time. Indeed, Ti/Al has previously been shown to reflect compositional changes in detrital fluxes to distal depositional sites through sea level fluctuations (Sageman et al. 2003).

Stage 2 (2100–700 BCE): Semi-open, lower salinity, improved bottom-water oxygen

During Stage 2, relative sea level was 7–12 m above present and because of isostatic regression Gåsfjärden began to evolve from an offshore system into a semi-open coastal basin with shallower water depth (Fig. 7). Declines of *Spiniferites* spp. and *L. machaerophorum* indicate lowered surface salinity. The gradual freshening in Gåsfjärden is synchronous with the open Baltic Sea, where the marine siliceous microfossil and dinoflagellate cysts also decreased (Andrén et al. 2000; Brenner 2005). The *O. centrocarpum* abundance exhibited a delayed response because this species is more tolerant of salinity variations than are *Spiniferites* spp. (Sildever et al. 2015).

The declines between 2100 and 700 BCE in the C_{org}, its MARs and C_{org}/P_{tot} ratios suggest decreased productivity and improving bottom-water oxygen conditions (Fig. 6). The transition from distinct light and dark bands to more homogenous sediments also suggests a change to improved bottom-water oxygen conditions, supporting the interpretation of C_{org}/P_{tot} ratios. The X-ray images reveal that even in the more homogenous sediments, laminae structures are still clearly visible (Fig. 4). This suggests that even though the oxygen conditions improved in this stage, benthic burrowing animals were still not well established, possibly because of seasonal hypoxia. K/Al and Ti/Al declined throughout Stage 2, reflecting changes in composition of the detrital flux during the embayment process, as in Stage 1. The increase in clay fractions indicates the depositional environment became calmer as Gåsfjärden became more enclosed.

Isostatic regression was not the only factor that could have driven the biogeochemical and ecological changes observed during Stage 2. Regional climate shifted to wetter and colder conditions from ca. 2000 BCE onwards, associated with the decline of the Holocene thermal maximum (HTM; Seppä et al. 2009). Annual and summer temperatures both decreased about 1 °C compared to the HTM (Seppä et al. 2009; Fig. 9). The colder conditions may have suppressed phytoplankton growth in general, as a result of a shorter growing season and reduced light intensity, caused by better water mixing under colder climate (Doney 2006; Sun et al. 2011). BSi content in Gåsfjärden exhibits a pattern similar to $\delta^{18}O$ measurements from Lake Blektjärnen (Andersson et al. 2010), suggesting a climatic influence on diatom production and deposition. In summary, reduced water depth, weakened stratification, together with a productivity decline, improved bottom-water oxygen conditions between 2100 and 700 BCE.

Stage 3 (700 BCE–600 CE): Relatively stable coastal environment

A major transition in both the geochemical and biological variables is observed at 700 BCE. The timing coincides with the sub-Boreal/sub-Atlantic climate boundary in Europe (Van Geel et al. 1996) and a shift to wetter regional conditions (Gałka et al. 2014; Hammarlund et al. 2003).

Low abundances of various dinoflagellate cyst species recorded at this stage suggest a continuous synchronization with the open Baltic Sea during the Littorina Sea phase (Andrén et al. 2000; Brenner 2005). Although salinity decreased further, the salinity (~ 8) was still slightly higher than at present, based on the higher abundance of *Spiniferites* spp.

Geochemical variables suggest a relatively stable environment in Gåsfjärden at this stage. Declines in C_{org} and BSi content seem to follow the climate shift to cooler and wetter conditions (Fig. 9). The C_{org}/P_{tot} values are consistently lower than in Zone GEO-A2, suggesting further improved oxygen conditions. Stabilized K/Al and Ti/Al indicate a weakened impact from sea level change on the transport of detrital material to the coring site.

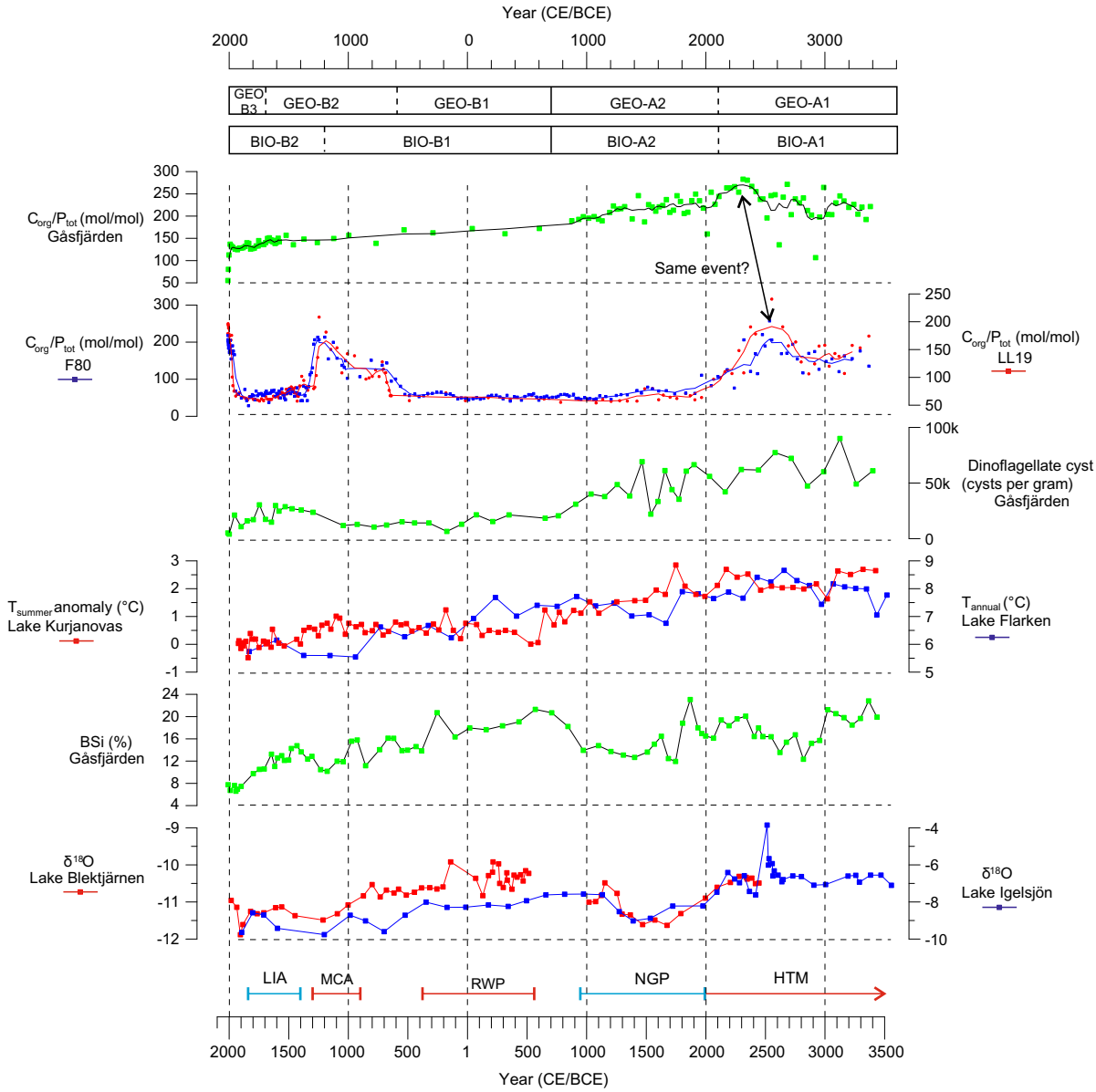

Fig. 9 Comparison of sediment variables from Gåsfjärden with regional climate reconstructions and C_{org}/P_{tot} records from the Gotland Basin area. Climate reconstructions include carbonate $\delta^{18}O$ records from Lake Igelsjön (Seppä et al. 2005) and Blektjärnen (Andersson et al. 2010), and pollen-based annual mean temperature and summer mean temperature reconstructions from Lake Flarken (Seppä et al. 2005) and Lake Kurjanovas (Heikkilä and Seppä 2010). Two C_{org}/P_{tot} records from LL19 and F80 in the Gotland Basin area (Jilbert and Slomp 2013) are compared. The C_{org}/P_{tot} records are shown with a 5-point running average. Climate episodes of the Holocene thermal maximum (HTM), Neoglacial Period (NGP), Roman Warm Period (RWP), Medieval Climate Anomaly (MCA) and Little Ice Age (LIA) are indicated based on Harland et al. (2013), Seppä et al. (2009) and Wang et al. (2012)

Stage 4 (600 CE–2011 CE): Strengthened human impact

Climate reconstructions indicate a shift to even cooler and wetter conditions over the last 2500 years (Andersson et al. 2010; McGregor et al. 2015), with two climate anomalies, the Medieval Climate Anomaly (MCA; 900–1300 CE) and the Little Ice Age (LIA; 1300–1850 CE; Fig. 9). Besides climate changes, land-use reconstruction based on pollen

analysis from Lake Storsjön, 25 km northwest of Gåsfjärden, indicates that intensified agriculture started in the region as early as 500 CE (unpublished data A. B. Nielsen). In addition, other pollen records from southern Sweden also show that forest clearance and grazing existed since 500 CE (Gaillard et al. 1994).

The increased abundance of the dinoflagellates *O. centrocarpum* and *P. psilata* between 1200 and 1950 CE, which includes the LIA, is unique, and a corresponding increase is not recorded in Gotland Basin (Brenner 2005). It is possible that the overall relatively minor increase in dinoflagellate cysts during the last 800 years, especially between 1200 and 1600 CE, is a more local response and reflects elevated nutrient input from the catchment.

The minor increases of C_{org}/N_{tot} and Ti/Al tend to support an inference for catchment disturbance since 600 CE. Rapid declines of C_{org} and BSi content between 1500 and 1950 CE coincide with increased Ti/Al ratios, indicating enhanced erosion, probably related to mining, industrial and agricultural activities in the catchment. A sharp increase of C_{org} after the 1950s is recorded in Gåsfjärden as well as in other Baltic regions, indicating the expansion of eutrophication (Jonsson and Carman 1994; Savage et al. 2010). BSi values do not increase in our record together with C_{org} values during the last few decades. Decoupling of BSi and C_{org} values was probably caused by a decline in periphytic diatoms as eutrophication intensified (Andrén et al. 1999). A shift from diatoms to dinoflagellates has also been observed in the Baltic Sea over the past three decades linked to relatively warm winters and changes in the mixed-layer depth (Wasmund and Uhlig 2003).

Comparing the hypoxia history of Gåsfjärden with deep basins of the Baltic Sea

Distinct dark and light bands in the sediment and high C_{org}/P_{tot} ratios demonstrate that frequent hypoxic conditions were present in Gåsfjärden from 3400 to 1000 BCE (Fig. 6). In the Baltic deep basins, hypoxic and anoxic bottom conditions generally prevailed between 3400 and 2000 BCE (Jilbert et al. 2015; Zillén et al. 2008), overlapping with the HTM period (Hammarlund et al. 2003; Renssen et al. 2009). The decline of hypoxic conditions at Gåsfjärden ca. 1000 BCE thus appears to occur later ($\sim$1000 years) than in the deep basins. The transition at Gåsfjärden ca. 1000 BCE is also far less pronounced than in the deep basins, where bottom water rapidly changed from hypoxic-anoxic to oxic conditions ca. 2000 BCE. A transition from laminated to homogenous sediments is also dated to ca. 1000 BCE in the Archipelago Sea (water depth 65 m; Virtasalo et al. 2006). This implies that in coastal regions where nutrient levels are higher than in the open sea, hypoxia tends to be more persistent. However, AMS ^{14}C dating of Baltic Sea bulk sediments, which has been widely applied to deep-basin sediment cores, could overestimate the real age by more than 1000 years (Kortekaas et al. 2007), and this potentially makes comparisons among sediment cores difficult.

Despite differences in the history of hypoxia among sites, our coastal record shares similarities with the records from the Gotland Basin area. The most intense hypoxic and anoxic period from our record is observed between 2800 and 2150 BCE, peaking around 2400–2100 BCE. In the Gotland Basin, the most intense hypoxic period over the last 6000 years is dated to between 2800 and 2300 BCE, with the peak at 2600–2400 BCE (Jilbert and Slomp 2013). The similar age of these severe hypoxia intervals indicates this is likely to have been a basin-wide event, linked to an extended period characterized by a highly productive and stratified water column. A carbonate $\delta^{18}O$ record from Lake Igelsjön shows a distinct warm and dry period between 2800 and 2200 BCE (Hammarlund et al. 2003; Fig. 9). The $\delta^{18}O$ and $\delta^{13}C$ records from Lake Blektjärnen in central Sweden also indicate dry and warm conditions between 2400 and 2200 BCE, with the peak at 2300 BCE (Andersson et al. 2010). A pollen-based temperature reconstruction from Lake Flarken indicates that the annual temperature was about 2 °C higher than present during this period (Seppä et al. 2005). Our dinoflagellate cyst record from Gåsfjärden shows high abundances of *L. machaerophorum* and *Spiniferites* spp. around 2300 BCE, indicating increased salinity, probably caused by decreased precipitation/runoff and increased evaporation under a relatively dry and warm climate. The development of anticyclonic blocking over the Scandinavian region, which leads to extended warm and dry summer conditions could explain the relatively high temperature ca. 2400–2300 BCE (Antonsson et al. 2008; Seppä et al. 2005). Furthermore, higher summer temperature and calm wind conditions favor

cyanobacteria blooms (Paerl and Huisman 2008), which are important sources of organic matter in the Gotland Basin (Struck et al. 2004). Therefore, a high C_{org}/P_{tot} at 2500–2300 BCE could partly be linked to cyanobacteria blooms, leading to hypoxic/anoxic bottom waters at Gåsfjärden and the Gotland Basin. Pigment analysis indicates high cyanobacteria concentrations in the Gotland Basin between 2800 and 2200 BCE, with maxima ca. 2500 BCE (Funkey et al. 2014).

In the Gotland Basin area, the reappearance of laminated sediments and redox proxies indicates that hypoxia-anoxia was re-established between 250 and 1250 CE, especially during the MCA period (Jilbert and Slomp 2013). Elevated sea surface temperature, together with population growth and land use changes were likely the main drivers of the hypoxic conditions and subsequent formation of laminated sediments during the MCA period (Kabel et al. 2012; Zillén et al. 2008). In contrast with the Arkona Basin and Gotland Basin, persistent hypoxia was not established in Gåsfjärden during the MCA period, because of the lack of a halocline and a shallower water depth. In the Bothnian Sea, continuous land uplift prevented water exchange with the open sea and the oxygenated bottom condition also prevailed during the MCA period (Jilbert et al. 2015).

Present hydrographic data from Gåsfjärden show seasonal hypoxia at a water depth of 20–25 m. Oxygen concentrations from 20 to 25 m water depth are most likely higher than at the coring site, which is located at 31 m water depth. Even more extensive hypoxia is expected in the deepest part (51 m) of Gåsfjärden. The sharp decline of C_{org}/P_{tot} in the uppermost part of the sediment core indicates that the surface sediment is currently retaining more phosphorus relative to carbon than before. This is largely a consequence of Fe-oxide-bound P, which accumulates in the surface sediment during seasons with oxygenated bottom water (data not shown). Such C_{org}/P_{tot} declines have also been recorded in surface sediments of the Bornholm Basin (Emeis et al. 2000) and Arkona Basin (Emeis et al. 2000; Mort et al. 2010).

Conclusions

Our multi-proxy study of the sediment record from Gåsfjärden highlights the response of this coastal environment to different drivers over the last 5400 years. Changes in climate, salinity, sea level, geomorphology and human activity were the key drivers of observed sedimentary changes and their individual importance has varied over time. It is likely that many other coastal sites in the Baltic Sea with relatively deep water experienced similar hypoxic-anoxic conditions during the middle to late Holocene, as observed at Gåsfjärden. Although Gåsfjärden had better exchange with the open sea between 3400 and 1000 BCE than during the latter period, a warmer and drier climate, greater water depth and more stratified water column led to the formation of frequent bottom-water hypoxia during that interval. Shoaling of the Baltic coastal zones, together with the decline in salinity, probably prevented extensive hypoxia during the Medieval Climate Anomaly, even though such conditions prevailed in the Baltic deep basins. The bottom water environment in Gåsfjärden has been subject to seasonal hypoxia for the last 20 years, as revealed by hydrographic measurements.

Acknowledgments We thank the captain and crew of *R/V Ocean Surveyor* for help during sampling. We thank Nathalie V. Putten and Åsa Wallin for guidance during grain size analysis. Anna Broström, Svante Björck, Anne Birgitte Nielsen and Conny Lenz are thanked for helpful discussions. Conny Lenz, Vincent Kofman and Leo de Jong assisted with sediment sampling and lab analysis. The project was funded by FORMAS Strong Research Environment: Managing Multiple Stressors in the Baltic Sea (217-2010-126). We also acknowledge funding from the Crafoord Foundation, the Royal Physiographic Society in Lund, and the Netherlands Organization for Scientific Research (NWO Vidi 86405.004 and ERC Starting Grant #278364). This work also resulted from the BONUS COCOA project supported by BONUS (Art 185), funded jointly by the EU and FORMAS. The hydrographic data used in the project were collected from SMHI's database-SHARK. The SHARK data collection is organized by the environmental monitoring program and funded by the Swedish Agency for Marine and Water Management (SWAM).

References

Algeo TJ, Ingall E (2007) Sedimentary C_{org}: P ratios, paleocean ventilation, and Phanerozoic atmospheric pO_2. Palaeogeogr Palaeoclimatol Palaeoecol 256:130–155

Al-Hamdani Z, Reker J (2007) Towards marine landscapes in the Baltic Sea. BALANCE interim report #10. http://balance-eu.org/

Andersen JH, Carstensen J, Conley DJ, Dromph K, Fleming-Lehtinen V, Gustafsson BG, Josefson AB, Norkko A, Villnäs A, Murray C (2015) Long-term temporal and

spatial trends in eutrophication status of the Baltic Sea. Biol Rev. doi:10.1111/brv.12221

Andersson S, Rosqvist G, Leng MJ, Wastegård S, Blaauw M (2010) Late Holocene climate change in central Sweden inferred from lacustrine stable isotope data. J Quat Sci 25:1305–1316

Andrén E, Shimmield G, Brand T (1999) Environmental changes of the last three centuries indicated by siliceous microfossil records from the southwestern Baltic Sea. Holocene 9:25–38

Andrén E, Andrén T, Kunzendorf H (2000) Holocene history of the Baltic Sea as a background for assessing records of human impact in the sediments of the Gotland Basin. Holocene 10:687–702

Anjar J, Larsen NK, Håkansson L, Möller P, Linge H, Fabel D, Xu S (2014) A 10Be-based reconstruction of the last deglaciation in southern Sweden. Boreas 43:132–148

Antonsson K, Chen D, Seppä H (2008) Anticyclonic atmospheric circulation as an analogue for the warm and dry mid-Holocene summer climate in central Scandinavia. Clim Past 4:585–610

Benninghoff WS (1962) Calculation of pollen and spore density in sediments by addition of exotic pollen in known quantities. Pollen Spores 4:332–333

Björck S (1995) A review of the history of the Baltic Sea, 13.0–8.0 ka BP. Quat Int 27:19–40

Blass A, Bigler C, Grosjean M, Sturm M (2007) Decadal-scale autumn temperature reconstruction back to AD 1580 inferred from the varved sediments of Lake Silvaplana (southeastern Swiss Alps). Quat Res 68:184–195

Bonsdorff E, Blomqvist EM, Mattila J, Norkko A (1997) Coastal eutrophication: causes, consequences and perspectives in the Archipelago areas of the northern Baltic Sea. Estuar Coast Shelf Sci 44(Suppl 1):63–72

Brenner WW (2005) Holocene environmental history of the Gotland Basin (Baltic Sea)—a micropalaeontological model. Palaeogeogr Palaeoclimatol Palaeoecol 220:227–241

Caballero-Alfonso AM, Carstensen J, Conley DJ (2015) Biogeochemical and environmental drivers of coastal hypoxia. J Mar Syst 141:190–199

Carstensen J, Andersen JH, Gustafsson BG, Conley DJ (2014a) Deoxygenation of the Baltic Sea during the last century. Proc Natl Acad Sci USA 111:5628–5633

Carstensen J, Conley D, Bonsdorff E, Gustafsson B, Hietanen S, Janas U, Jilbert T, Maximov A, Norkko A, Norkko J, Reed D, Slomp C, Timmermann K, Voss M (2014b) Hypoxia in the Baltic Sea: biogeochemical cycles, benthic fauna, and management. Ambio 43:26–36

Conley DJ, Carstensen J, Ærtebjerg G, Christensen PB, Dalsgaard T, Hansen JLS, Josefson AB (2007) Long-term changes and impacts of hypoxia in Danish coastal waters. Ecol Appl 17:S165–S184

Conley DJ, Björck S, Bonsdorff E, Carstensen J, Destouni G, Gustafsson BG, Hietanen S, Kortekaas M, Kuosa H, Markus Meier HE, Müller-Karulis B, Nordberg K, Norkko A, Nürnberg G, Pitkänen H, Rabalais NN, Rosenberg R, Savchuk OP, Slomp CP, Voss M, Wulff F, Zillén L (2009) Hypoxia-related processes in the Baltic Sea. Environ Sci Technol 43:3412–3420

Conley DJ, Carstensen J, Aigars J, Axe P, Bonsdorff E, Eremina T, Haahti B-M, Humborg C, Jonsson P, Kotta J, Lännegren C, Larsson U, Maximov A, Medina MR, Lysiak-Pastuszak E, Remeikaitė-Nikienė N, Walve J, Wilhelms S, Zillén L (2011) Hypoxia is increasing in the coastal zone of the Baltic Sea. Environ Sci Technol 45:6777–6783

Dale B (1996) Dinoflagellate cyst ecology: modelling and geological applications. AASP Foundation, Dallas

Deflandre G, Cookson IC (1955) Fossil microplankton from Australian late Mesozoic and Tertiary sediments. Mar Freshw Res 6:242–314

DeMaster DJ (1981) The supply and accumulation of silica in the marine environment. Geochim Cosmochim Acta 45:1715–1732

Diaz RJ, Rosenberg R (2008) Spreading dead zones and consequences for marine ecosystems. Science 321:926–929

Doney SC (2006) Oceanography: plankton in a warmer world. Nature 444:695–696

Emeis KC, Struck U, Leipe T, Pollehne F, Kunzendorf H, Christiansen C (2000) Changes in the C, N, P burial rates in some Baltic Sea sediments over the last 150 years—relevance to P regeneration rates and the phosphorus cycle. Mar Geol 167:43–59

Emel'yanov EM, Luksha VL (2014) The clay mineralogy and paleogeography of the Gotland Basin (based on the data from the Psd-303590 core). Mosc Univ Geol Bull 69:219–228

Funkey CP, Conley DJ, Reuss NS, Humborg C, Jilbert T, Slomp CP (2014) Hypoxia sustains cyanobacteria blooms in the Baltic Sea. Environ Sci Technol 48:2598–2602

Gaillard MJ, Birks HJB, Emanuelsson U, Karlsson S, Lagerås P, Olausson D (1994) Application of modern pollen/land-use relationships to the interpretation of pollen diagrams—reconstructions of land-use history in south Sweden, 3000–0 BP. Rev Palaeobot Palynol 82:47–73

Gałka M, Miotk-Szpiganowicz G, Marczewska M, Barabach J, van der Knaap WO, Lamentowicz M (2014) Palaeoenvironmental changes in Central Europe (NE Poland) during the last 6200 years reconstructed from a high-resolution multi-proxy peat archive. Holocene 25:421–434

Gingele FX, Leipe T (1997) Clay mineral assemblages in the western Baltic Sea: recent distribution and relation to sedimentary units. Mar Geol 140:97–115

Grimm EC (1987) CONISS: a FORTRAN 77 program for stratigraphically constrained cluster analysis by the method of incremental sum of squares. Comput Geosci 13:13–35

Gustafsson BG, Westman P (2002) On the causes for salinity variations in the Baltic Sea during the last 8500 years. Paleoceanography 17:12-11–12-14

Gustafsson BG, Schenk F, Blenckner T, Eilola K, Meier HEM, Müller-Karulis B, Neumann T, Ruoho-Airola T, Savchuk O, Zorita E (2012) Reconstructing the development of Baltic Sea eutrophication 1850–2006. Ambio 41:534–548

Hammarlund D, Björck S, Buchardt B, Israelson C, Thomsen CT (2003) Rapid hydrological changes during the Holocene revealed by stable isotope records of lacustrine carbonates from Lake Igelsjön, southern Sweden. Quat Sci Rev 22:353–370

Harland R, Polovodova Asteman I, Nordberg K (2013) A two-millennium dinoflagellate cyst record from Gullmar Fjord,

a Swedish Skagerrak sill fjord. Palaeogeogr Palaeoclimatol Palaeoecol 392:247–260
Head MJ (1994) Morphology and paleoenvironmental significance of the Cenozoic dinoflagellate genera *Tectatodinium* and *Habibacysta*. Micropaleontology 40:289–321
Heikkilä M, Seppä H (2010) Holocene climate dynamics in Latvia, eastern Baltic region: a pollen-based summer temperature reconstruction and regional comparison. Boreas 39:705–719
HELCOM (2009) Eutrophication in the Baltic Sea—an integrated thematic assessment of the effects of nutrient enrichment and eutrophication in the Baltic Sea region. http://www.helcom.fi/
Hermelin JOR (1987) Distribution of Holocene benthic foraminifera in the Baltic Sea. J Foraminiferal Res 17:62–73
Jilbert T, Slomp CP (2013) Rapid high-amplitude variability in Baltic Sea hypoxia during the Holocene. Geology 41:1183–1186
Jilbert T, Conley DJ, Gustafsson BG, Funkey CP, Slomp CP (2015) Glacio-isostatic control on hypoxia in a high-latitude shelf basin. Geology. doi:10.1130/g36454.1
Jonsson P, Carman R (1994) Changes in deposition of organic matter and nutrients in the Baltic Sea during the twentieth century. Mar Pollut Bull 28:417–426
Juggins S (2014) rioja: an R package for the analysis of quaternary science data. http://cran.r-project.org/package=rioja
Kabel K, Moros M, Porsche C, Neumann T, Adolphi F, Andersen TJ, Siegel H, Gerth M, Leipe T, Jansen E, Sinninghe Damste JS (2012) Impact of climate change on the Baltic Sea ecosystem over the past 1,000 years. Nat Clim Change 2:871–874
Karlsson J, Segerström U, Berg A, Mattielli N, Bindler R (2015) Tracing modern environmental conditions to their roots in early mining, metallurgy, and settlement in Gladhammar, southeast Sweden: vegetation and pollution history outside the traditional Bergslagen mining region. Holocene 25:944–955
Kortekaas M, Murray AS, Sandgren P, Björck S (2007) OSL chronology for a sediment core from the southern Baltic Sea: a continuous sedimentation record since deglaciation. Quat Geochronol 2:95–101
Kotilainen A, Vallius H, Ryabchuk D (2007) Seafloor anoxia and modern laminated sediments in coastal basins of the Eastern Gulf of Finland, Baltic Sea. Special Paper of the Geological Survey of Finland, pp 49–62
Legrand C, Fridolfsson E, Bertos-Fortis M, Lindehoff E, Larsson P, Pinhassi J, Andersson A (2015) Interannual variability of phyto-bacterioplankton biomass and production in coastal and offshore waters of the Baltic Sea. Ambio 44:427–438
Leppäranta M, Myrberg K (2009) Physical oceanography of the Baltic Sea. Springer, New York
Lougheed BC, Filipsson HL, Snowball I (2013) Large spatial variations in coastal 14C reservoir age—a case study from the Baltic Sea. Clim Past 9:1015–1028
McGregor HV, Evans MN, Goosse H, Leduc G, Martrat B, Addison JA, Mortyn PG, Oppo DW, Seidenkrantz M-S, Sicre M-A, Phipps SJ, Selvaraj K, Thirumalai K, Filipsson HL, Ersek V (2015) Robust global ocean cooling trend for the pre-industrial Common Era. Nat Geosci 8:671–677
Meyers PA (1994) Preservation of elemental and isotopic source identification of sedimentary organic matter. Chem Geol 114:289–302
Mort HP, Slomp CP, Gustafsson BG, Andersen TJ (2010) Phosphorus recycling and burial in Baltic Sea sediments with contrasting redox conditions. Geochim Cosmochim Acta 74:1350–1362
Nehring D, Matthäus W, Lass H-U, Nausch G, Nagel K (1995) The Baltic Sea in 1995—beginning of a new stagnation period in its central deep waters and decreasing nutrient load in its surface layer. Dtsch Hydrogr Z 47:319–327
Ning W, Andersson PS, Ghosh A, Khan M, Filipsson HL (2015) Quantitative salinity reconstructions of the Baltic Sea during the mid-Holocene. Boreas. doi:10.1111/bor.12156
Paerl HW, Huisman J (2008) Blooms like it hot. Science 320:57–58
Påsse T, Andersson L (2005) Shore-level displacement in Fennoscandia calculated from empirical data. GFF 127:253–268
Persson J, Jonsson P (2000) Historical development of laminated sediments—an approach to detect soft sediment ecosystem changes in the Baltic Sea. Mar Pollut Bull 40:122–134
Pospelova V, Esenkulova S, Johannessen SC, O'Brien MC, Macdonald RW (2010) Organic-walled dinoflagellate cyst production, composition and flux from 1996 to 1998 in the central Strait of Georgia (BC, Canada): a sediment trap study. Mar Micropaleontol 75:17–37
Ramsey CB (2008) Deposition models for chronological records. Quat Sci Rev 27:42–60
Redfield AC (1963) The influence of organisms on the composition of sea-water. In: Hill MN (ed), The sea, vol 2. Interscience, New York, pp 26–77
Reid P (1974) Gonyaulacacean dinoflagellate cysts from the British Isles. Nova Hedwig 25:579–637
Renssen H, Seppä H, Heiri O, Roche DM, Goosse H, Fichefet T (2009) The spatial and temporal complexity of the Holocene thermal maximum. Nat Geosci 2:411–414
Rochon A, Vernal Ad, Turon J-L, Matthießen J, Head M (1999) Distribution of recent dinoflagellate cysts in surface sediments from the North Atlantic Ocean and adjacent seas in relation to sea-surface parameters. Am Assoc Strat Palynol Contrib Ser 35:1–146
Rolff C, Almesjö L, Elmgren R (2007) Nitrogen fixation and abundance of the diazotrophic cyanobacterium *Aphanizomenon* sp. in the Baltic proper. Mar Ecol Prog Ser 332:107–118
Sageman BB, Murphy AE, Werne JP, Ver Straeten CA, Hollander DJ, Lyons TW (2003) A tale of shales: the relative roles of production, decomposition, and dilution in the accumulation of organic-rich strata, Middle-Upper Devonian, Appalachian basin. Chem Geol 195:229–273
Savage C, Leavitt PR, Elmgren R (2010) Effects of land use, urbanization, and climate variability on coastal eutrophication in the Baltic Sea. Limnol Oceanogr 55:1033
Seppä H, Hammarlund D, Antonsson K (2005) Low-frequency and high-frequency changes in temperature and effective humidity during the Holocene in south-central Sweden: implications for atmospheric and oceanic forcings of climate. Clim Dyn 25:285–297

Seppä H, Bjune A, Telford R, Birks H, Veski S (2009) Last nine-thousand years of temperature variability in Northern Europe. Clim Past 5:523–535

Sildever S, Andersen TJ, Ribeiro S, Ellegaard M (2015) Influence of surface salinity gradient on dinoflagellate cyst community structure, abundance and morphology in the Baltic Sea, Kattegat and Skagerrak. Estuar Coast Shelf Sci 155:1–7

SMHI (2003) Djupdata för havsområden 2003. Oceanografi, Norrköping

Söderhielm J, Sundblad K (1996) The Solstad Cu–Co–Au mineralization and its relation to post-Svecofennian regional shear zones in southeastern Sweden. GFF 118:47

Stephens M, Ripa M, Lundström I, Wickström L (2009) Synthesis of the bedrock geology in the Bergslagen region, Fennoscandian shield, south-central Sweden. Publication Ba58, Swedish Geological Survey, Uppsala, 259 pp

Struck U, Pollehne F, Bauerfeind E, von Bodungen B (2004) Sources of nitrogen for the vertical particle flux in the Gotland Sea (Baltic Proper)—results from sediment trap studies. J Mar Syst 45:91–101

Sun X, Andersson P, Humborg C, Gustafsson B, Conley DJ, Crill P, Mörth CM (2011) Climate dependent diatom production is preserved in biogenic Si isotope signatures. Biogeosciences 8:3491–3499

Vahtera E, Conley DJ, Gustafsson BG, Kuosa H, Pitkänen H, Savchuk OP, Tamminen T, Viitasalo M, Voss M, Wasmund N (2007) Internal ecosystem feedbacks enhance nitrogen-fixing cyanobacteria blooms and complicate management in the Baltic Sea. Ambio 36:186–194

Van Geel B, Buurman J, Waterbolk HT (1996) Archaeological and palaeoecological indications of an abrupt climate change in The Netherlands, and evidence for climatological teleconnections around 2650 BP. J Quat Sci 11:451–460

Van Hengstum PJ, Reinhardt EG, Boyce JI, Clark C (2007) Changing sedimentation patterns due to historical land-use change in Frenchman's Bay, Pickering, Canada: evidence from high-resolution textural analysis. J Paleolimnol 37:603–618

Van Santvoort PJM, De Lange GJ, Thomson J, Colley S, Meysman FJR, Slomp CP (2002) Oxidation and origin of organic matter in surficial eastern Mediterranean hemipelagic sediments. Aquat Geochem 8:153–175

Verardo DJ, Froelich PN, McIntyre A (1990) Determination of organic carbon and nitrogen in marine sediments using the Carlo Erba NA-1500 Analyzer. Deep Sea Res A 37:157–165

Virtasalo JJ, Kotilainen AT, Gingras MK (2006) Trace fossils as indicators of environmental change in Holocene sediments of the Archipelago Sea, northern Baltic Sea. Palaeogeogr Palaeoclimatol Palaeoecol 240:453–467

Virtasalo JJ, Leipe T, Moros M, Kotilainen AT (2011) Physicochemical and biological influences on sedimentary-fabric formation in a salinity and oxygen-restricted semi-enclosed sea: Gotland Deep, Baltic Sea. Sedimentology 58:352–375

Wall D, Dale B (1968) Modern dinoflagellate cysts and evolution of the peridiniales. Micropaleontology 14:265–304

Wang T, Surge D, Mithen S (2012) Seasonal temperature variability of the Neoglacial (3300–2500 BP) and Roman Warm Period (2500–1600 BP) reconstructed from oxygen isotope ratios of limpet shells (Patella vulgata), Northwest Scotland. Palaeogeogr Palaeoclimatol Palaeoecol 317–318:104–113

Wasmund N, Uhlig S (2003) Phytoplankton trends in the Baltic Sea. ICES J Mar Sci 60:177–186

Wehausen R, Brumsack H-J (2000) Chemical cycles in Pliocene sapropel-bearing and sapropel-barren eastern Mediterranean sediments. Palaeogeogr Palaeoclimatol Palaeoecol 158:325–352

Widerlund A, Andersson PS (2011) Late Holocene freshening of the Baltic Sea derived from high-resolution strontium isotope analyses of mollusk shells. Geology 39:187–190

Willumsen PIS, Filipsson HL, Reinholdsson M, Lenz C (2013) Surface salinity and nutrient variations during the Littorina Stage in the Fårö Deep, Baltic Sea. Boreas 42:210–223

Yu S-Y, Berglund BE (2007) A dinoflagellate cyst record of Holocene climate and hydrological changes along the southeastern Swedish Baltic coast. Quat Res 67:215–224

Zalewska T, Suplińska M (2013) Anthropogenic radionuclides ^{137}Cs and ^{90}Sr in the southern Baltic Sea ecosystem. Oceanologia 55:485–517

Zillén L, Conley DJ, Andrén T, Andrén E, Björck S (2008) Past occurrences of hypoxia in the Baltic Sea and the role of climate variability, environmental change and human impact. Earth Sci Rev 91:77–92

Zonneveld KAF, Chen L, Elshanawany R, Fischer HW, Hoins M, Ibrahim MI, Pittauerova D, Versteegh GJM (2012) The use of dinoflagellate cysts to separate human-induced from natural variability in the trophic state of the Po River discharge plume over the last two centuries. Mar Pollut Bull 64:114–132